# Light bending and the hard X-ray background

P. Gandhi

Institute of Physical and Chemical Research (RIKEN), 2-1 Hirosawa, Wakoshi, Saitama 351-0198, Japan
*E-mail: pg@crab.riken.jp*

Abstract

Light bending due to strong gravity has recently been invoked to explain variability and flux correlations between different bands in some accreting black holes. A characteristic feature of light bending is reflection-dominated spectra, especially if photon sources lie in the deepest parts of the gravitational potential within a few gravitational radii of the event horizon. We use the spectrum of the hard X-ray background in order to constrain the prevalence of such reflection-dominated sources. We first explore the broad-band properties of realistic spectra that incorporate light bending and then use these spectra, in conjunction with the observed 2–10 keV AGN luminosity functions in order to predict the hard X-ray background spectrum over 3–100 keV, and provide limits on the fraction of reflection-dominated sources, dependent on the flare height. Our results allow for a cosmologically- significant fraction of sources that incorporate strong light bending. The luminosity function based on intrinsic flare luminosities is derived. We discuss prospects for missions such as *NeXT* and *Simbol-X* that can image such sources as well as confirm the precise spectral shape of the background near its peak, important for constraining the universal relevance of light bending.

Key words: galaxies: active – X-rays: galaxies – X-rays: cosmic background radiations

## 1. Introduction

We pose a simple question: How common are active galactic nuclei (AGN) with extreme reflection fractions in X-rays? The motivation for this is the recent finding that incorporation of general relativistic light bending effects on photon propagation can have dramatic consequences for the spectra of accreting sources with peaked central emissivities. For isotropic photon sources (such as magnetic reconnection events/flares, a hot electron corona or the base of a jet) that lie within a few gravitational radii ($R_{\rm G} = GM_{\rm BH}/c^2$) of the BH, the cross-section of photon geodesics intercepting the accretion disk (or lost down the event horizon) can be very large, as compared to sources at much higher heights ($h$). For constant luminosity photon sources, the primary flux observed at infinity can vary dramatically with changing source height, while the reflected flux component remains relatively unchanged, resulting in reflection-dominated spectra for low $h$. This model has been shown to be capable of explaining the apparently dis-jointed variability patterns and flux-flux correlations observed between different bands in some Seyferts, Narrow Line Seyfert 1s, as well as Galactic BH candidates (e.g., Miniutti & Fabian 2004, Fabian et al. 2005, Rossi et al. 2005, Ponti et al. 2006).

The general importance of the light bending model is currently unclear, though evidence for sources with high reflection fractions (e.g. Panessa et al. 2008, Ueda et al. 2007) is increasing; as is evidence for the ubiquity of rapidly-spinning black holes with accretion disks extending down to the innermost stable circular orbits, where light bending should be strongest (Fabian et al. 2002, Volonteri et al. 2005, Wang et al. 2006).

In this work, we use the cosmological hard X-ray background (XRB) radiation to place constraints on the fraction of sources which are reflection-dominated. This is possible because the background is simply the integrated emission of AGN spread out in redshift, and its characteristic spectral shape irrefutably requires the presence of reflection. Full details have been published in Gandhi et al. (2007).

## 2. Reflection-dominated AGN spectra

As our base broad-band spectral energy distributions (SEDs), we use the ones of Suebsuwong et al. (2006; hereafter S06), who have carried out detailed Monte Carlo investigations that incorporate light bending to quantify changes in observed spectral properties, with the variables being inclination angle, source height, source size (either point-like or ring-like) and source distance from the rotation axis, assuming the proper Kerr space-time metric and no emission from the plunging region between the innermost marginally stable orbit of the accretion flow and the event horizon. The specific angular momentum of the BH is taken to be $a = 0.998$, implying that the innermost stable orbit lies at a distance

of 1.23 $R_{\rm G}$ from the BH. For simplicity, we consider only the case with on-axis point-like flares at height $h$ above the accretion disk.

Fig. 1 shows the effect of increasing light bending from bottom-to-top. The 'PEXRAV' SED is taken to be the unabsorbed template SED used by Gandhi & Fabian (2003): a power-law with a photon-index ($\Gamma$) of 1.9 and a reflection component from a flat, infinite slab covering $2\pi$ steradians viewed at an inclination angle ($i$) of 60 degs, generated according to Magdziarz & Zdziarski (1995). An exponential power-law cut-off ($E_{\rm cut}$)=500 keV is used, in order to directly compare with the results of Ueda et al. (2003, hereafter U03). The spectra that incorporate light-bending are plotted for a range of source heights (S06 generate spectra at four discrete heights of $h = 2, 5, 10$ and 20 $R_{\rm G}$). For the present comparison, these spectra have been averaged over all viewing angles, and are normalized at 1 keV. Identical intrinsic $\Gamma$ and $E_{\rm cut}$ values are assumed in all the spectra plotted in the figure, including the reflection-free power-law ('PL').

As source height decreases from bottom-to-top, more photons are bent towards the central object, and also impinge on the accretion disk, resulting in a larger reflection fraction. For the lowest height plotted ($h = 2$), the peak monochromatic flux is higher than that of the PEXRAV SED by a factor of 26 (6), for a normalization at 1 keV (over 2–10 keV). As $h$ increases, the photon source is located in regions of shallower gravitational potential and the effect of light bending decreases until, for $h = 20$, the reflection fraction closely matches the PEXRAV $2\pi$ reflector model.

To summarize, the result of an increased reflection component is that the spectra become more 'peaky' in $EF_E(\equiv \nu F_\nu)$ units.

Fig. 2 shows a schematic illustration of the actual reflection model that we envision. Light bending enhances the disk reflection component, which may subsequently be obscured by the torus along the observed line-of-sight, depending on inclination angle. A more distant reflection component may be attributed to the inner torus walls and result in a narrow Fe emission line; this component is likely to be unabsorbed.

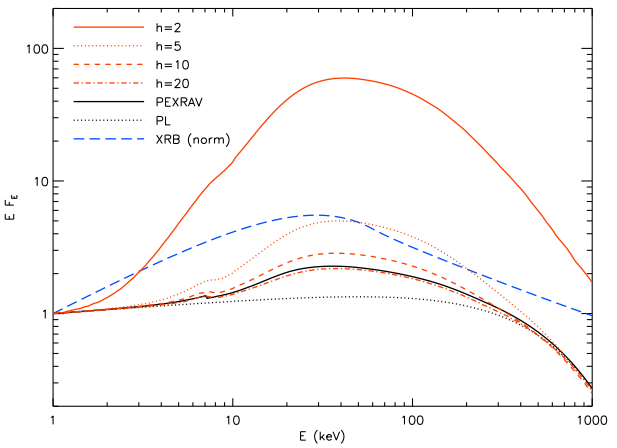


Fig. 1. Comparison of angle-averaged broad-band light-bending SEDs (source height as labelled) with a PEXRAV ($R = 1$; $\theta = 60$ degs; solid black) and simple cut-off power-law (PL; no reflection; lowest dotted black) SEDs. All spectra assume an incident power-law with $\Gamma = 1.9$ and an exponential cut-off $E_{\rm cut} = 500$ keV, and have been normalized at 1 keV. The observed XRB fit from Gruber et al. (1999), also similarly normalized, is shown as the blue long-dashed line.

## 3. Distributions in luminosity and obscuring column

In order to simulate the X-ray background (XRB) spectrum, we require a distribution of sources in luminosity and obscuration parameter space. One of the best-determined X-ray luminosity functions (XLF) and $N_{\rm H}$ distributions is that of U03 over the 2–10 keV range, which we use here until more precise measurements become available above 10 keV from on-going *Swift* and *INTEGRAL* surveys. We use the luminosity-dependent density evolution (LDDE) in redshift model favoured by U03.

A range of obscured reflection-dominated spectra were generated, with columns of cold gas ranging from log$N_{\rm H}$=20–22 for Sy 1s (intrinsic spectrum averaged over viewing angles of 0–50 degs) and log$N_{\rm H}$=22–25 (Sy 2s; averaged over 50–90 degs), for each height $h$. For Compton-thick sources, the effects of down-scattering (Wilman & Fabian 1999) were fully included.

Fits to the XRB are carried out over the 3–100 keV range by assuming that the *HEAO* error bars are normally-distributed, and computing a weighted sum of square deviations (an effective '$\chi^2$'). The difference in this fit parameter ($\Delta\chi^2$) is computed relative to the base U03 model (without inclusion of light bending). Given the uncertainty in the population size of Compton-thick sources, we allow the fractional contribution of Compton-thick AGN (log$N_{\rm H}$=24–25) to vary by a factor of $0 \leq r_{\rm CT} \leq 2$, where $r_{\rm CT} = 1$ represents an equal normalization between Compton-thick sources and Compton-thin ones with log$N_{\rm H}$=23–24, as assumed by U03. Finally, in order to account for uncertainties in the XLF (at least 5 per cent) as well as the shape and normalization of the XRB itself (e.g., Ajello et al. 2008), we allow a final variable normalization of between 0.95 and 1.05 applied to the overall spectrum.

Any realistic AGN population is likely to have a mixture of sources that readily show light bending, and those that do not. We thus assume that light bending is important in a certain fixed fraction ($f$) of all AGN, and we produce results for various values of $f$.

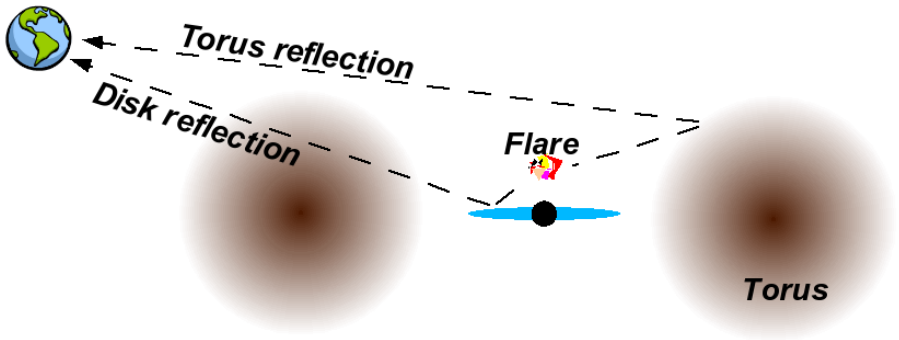


Fig. 2. Schematic picture showing the two reflection components in our AGN SEDs. Light bending strongly enhances the disk reflection component, for low heights $h$ of flares above the event horizon. Depending on the angle of inclination, this component may be absorbed along the line-of-sight through the torus. Torus reflection is generically imagined to be unabsorbed.

## 4. Results

Although the torus reflection component is an integral part of our model, in order to clearly gauge the effect of the light bending, we separated our fits into two classes: those with a torus reflection component (so the overall SEDs have a fraction $f$ of sources with PEXRAV+light bending included, and a factor $1-f$ of PEXRAV only), and those without (i.e. a simple PL, instead of the torus PEXRAV). With respect to the schematic of Fig. 2, this is equivalent to determining the fraction of sources in which only light-bent disk reflection component contributes significantly to the overall SED, as opposed to the torus, or other reflection components.

Fig. 3 shows the improvement in $\chi^2$ (with respect to the base model of U03) of the various fits to the XRB spectrum using the reflection-dominated SEDs. For spectra with a particular flare height $h$, various values of the light bending $f$ were tried, and the maximum change in $\chi^2$ is plotted. As an example, the XRB spectrum solution for one of the best models with $h = 5$ and a 30 % contribution of light bending ($f = 0.3$) is shown to reproduce the background data very well.

Compiling all our results, we are now immediately able to answer the question that we posed at the beginning. The overall prevalence of sources with light bending is shown in Fig. 4, as a function of source flare height.

## 5. Discussion

Our results show that the XRB allows for the existence of a significant fraction of sources with pronounced light bending. Assuming that light bending is important in a certain fraction ($f$) of sources, we derive broad constraints on $f$ by fitting the hard X-ray background over 3–100 keV. $f$ can be thought of as representing the distribution of sources with high effective reflection fractions ($R > 1$). Including both PEXRAV and light bending reflection components, we find values $f \leq 0.02, 0.1$ and 0.5 (decreasing with decreasing source height $h$ [or equivalently, with increasing spectrum peakiness]; Fig. 3, *top*). Slightly larger values of $f$ can be allowed if the peaky contribution of Compton-thick sources is neglected, though it is likely that a sizable fraction of Compton-thick AGN exists in the Universe. If light bending is the only source of reflection (the 'PL+light bending' scenario; Fig. 3, *middle*), then specific ranges of $f \approx 0.05 (h = 2), 0.1 - 0.3 (h = 5)$ and $0.3 - 0.8 (h = 10)$ are required, due to the fact that reflection-free SEDs under-predict the XRB peak. Fig. 4 has summarized all the allowed solutions in one place.

In Gandhi et al. (2007), a number of consequences of our findings have been discussed. These include the effects of ionized reflection (Ross & Fabian 2005) as may be expected within the innermost hot accretion flow regions, and the possibility of fitting the X-ray background without a significant Compton-thick population, if light-bent spectra can instead provide the peakiness required by the XRB spectrum. Here we discuss two other important aspects: that the total accretion power released in the Universe may have to be significantly increased, and the implied detectability of light-bent sources with upcoming missions.

### 5.1. Higher intrinsic flare luminosities

The U03 XLF involves the intrinsic 2–10 keV luminosity ($L_{2-10}$) and inherently assumes that this can be computed by correction of the observed source flux for obscuration and redshift effects only. On the other hand, one of the main conclusions of Miniutti & Fabian (2004) was that, under the light bending scenario, variations in the height of a flare of constant luminosity could cause the observed primary power-law emission to vary dramatically (while leaving the reflected component largely unchanged). For properly 'flux-calibrated' spectra determined by S06 (see their Figs. 6a and 15), the flux seen at infinity decreases with decreasing flare height (with

a dependence on the inclination angle) due to multiple reflections, scattering, gravitational redshifting and photons falling into the event horizon. If one knows the flux loss factor, then one can correct these to determine the intrinsic flare luminosities ($L_{\rm flare}$). For the modelled Monte Carlo light-bent spectra, it is possible to compute that for $h = 2, 5$ and 10, the inferred 2–10 keV luminosity at infinity is 0.02, 0.17 and 0.36 times $L_{\rm flare}$, due to the effect of light bending. Combining this flux loss per AGN with the best-fit light bending contribution ($f$), the XLF ($d\Phi/d\log L_{\rm flare}$) based on intrinsic flare luminosities can be computed. This is shown in Fig. 5.

Clearly, our corrections imply a larger number density (per cubic comoving Mpc) at the same luminosity, in the case of stronger light bending. This number density can exceed the XLF without light bending by a factor of between $\sim 5$ and 160 for the PEXRAV+light bending case shown (and even more for the PL+light bending case); the largest excess being at highest luminosities due to the steep slope of the XLF there. Since $f$ is taken to be independent of $z$, similar behaviour is expected at higher redshift, with the exact deviation from the base XLF depending on its slope.

AGN Eddington fractions would then also be correspondingly increased (for a constant black hole mass). On a cosmological scale, using our results would imply that local Seyferts should have mean Eddington ratios larger by a maximum factor of $\sim 1.5 - 6$ (when averaged over all $\log L < 44.5$), while the corresponding increase for higher luminosity quasars should be $\sim 5 - 500$. The above increase in mean Eddington ratios is comparatively modest (at least for Seyferts), and has already been inferred for at least one source (Miniutti et al. 2007).

Interestingly, flux loss down the event horizon should also be strong enough to increase the local mass density in black holes by up to 14% in the case of extreme light bending (see details in Gandhi et al. 2007).

### 5.2. Predictions for hard X-ray missions

On-going surveys with *INTEGRAL* and *Swift* (Beckmann et al. 2006, Markwardt et al. 2005) should begin to detect sources in which light bending dominates, if these sources occur at low redshift and low-luminosity. Some will also definitely be detected by *MAXI* (e.g., Matsuoka et al. 2007), though measuring accurate reflection fractions may have to await telescopes such as *NeXT* and *Simbol-X*.

The large hard X-ray effective area design of *NeXT* will give a continuum sensitivity of several $\times 10^{-8}$ photons s$^{-1}$ keV$^{-1}$ cm$^{-2}$ in 100 ks, or a point-source flux limit of $\sim 5.0, 1.7$ and $0.6 \times 10^{-14}$ erg s$^{-1}$ cm$^{-2}$ over 8–80, 20–50 and 10–30 keV respectively, assuming a power-law source with a photon-index of 2 (the exact sensitivity depends on the final telescope configuration parameters, which are to be finalized in the near future). At these flux limits, 35, 39 and 68 per cent of the total XRB in the respective bands will be resolved, for the XRB normalization adopted by U03. If the original XRB normalization due to Gruber et al. is closer to the correct value, the above percentages will be increased by a factor of 1.26.

As an example, in Fig. 6 we show (as the thick lines) the cumulative XRB expected to be resolved by *NeXT* in the 8–80 keV band, along with the corresponding cumulative number counts as a function of flux. For this illustration, we chose one of the good solutions with the maximum allowed $f$ value (in this case, $f = 0.3$ for $h = 5$ for the 'PL+light bending' scenario; cf. the bottom plots of Fig. 3) in order to show the effect of light bending. Compared to the currently resolved XRB level of $\sim 1\%$ over this energy range, the next generation of hard X-ray telescopes will enable us to make a quantum leap in knowledge.

## 6. Conclusions

Our results allow for a cosmologically-significant fraction of sources that are reflection dominated. The percentage of AGN in which strong light bending is occurring may be anywhere between 2 and 50% of all AGN, depending on source flare height. One of the important implications of this is that the total accretion energy density released in the Universe must be larger (on average, by a factor of a few) because only a fraction of the released accretion energy is actually observed at infinity. Such sources should be observable by the next generation of hard X-ray missions.

P.G. acknowledges a Fellowship of the Japan Society for the Promotion of Science during the course of this work. He warmly thanks the organizers for an interesting meeting.

## References

Ajello M. et al. 2008 ApJ. in press, arXiv:astro-ph/0808.3377

Beckmann V., Gehrels N., Shrader C.R. & Soldi S. 2006 ApJ., 638, 642

Fabian A.C. et al. 2002 MNRAS., 335, L1

Fabian A.C., Miniutti G., Iwasawa K. & Ross R.R. 2005 MNRAS., 361, 795

Frontera F. et al. 2007 ApJ., 666, 86

Gandhi P. & Fabian A.C. 2003 MNRAS., 339, 1095

Gandhi P. et al. 2007 MNRAS., 382, 1005

Gruber D.E., Matteson J.L., Peterson L.E. & Jung G.V. 1999 ApJ., 520, 124

Matsuoka M. et al. 2007 in Society of Photo-Optical Instrumentation Engineers (SPIE) Conference, Vol.

6686, UV, X-Ray, and Gamma-Ray Space Instrumentation for Astronomy XV. Edited by Siegmund, Oswald H. Proceedings of the SPIE, Volume 6686, pp. 668611-668611-9 (2007)
Magdziarz P. & Zdziarski A.A., 1995, MNRAS., 273, 837
Miniutti G. & Fabian A.C. 2004 MNRAS., 349, 1435
Miniutti G. et al. 2007 MNRAS., 375, 227
Panessa F. et al. 2008 A&A., 483, 151
Ponti G. et al. 2006 MNRAS., 368, 903
Ross R.R. & Fabian A.C. 2005 MNRAS., 261, 74
Rossi S., Homan J., Miller J.M. & Belloni T. 2005 MNRAS., 360, 763
Suebsuwong T. et al. 2006 A&A., 453, 773 **(S06)**
Takahashi T., Mitsuda K., Kunieda H. 2006 in Turner M. J. L., Hasinger G., ed, Space Telescopes and Instrumentation II: Ultraviolet to Gamma Ray. Edited by Turner, Martin J. L.; Hasinger, Günther. Proceedings of the SPIE, Volume 6266, pp. 62660D (2006)
Ueda Y. et al. 2003 ApJ., 598, 886 **(U03)**
Ueda Y. et al. 2007 ApJ., 664, L79
Volonteri M., Madau P., Quataert E. & Rees M.J. 2006 ApJ., 620, 69
Wang J.-M. et al. 2006 ApJ., 642, L111
Wilman R.J. & Fabian A.C. 1999 MNRAS., 309, 862

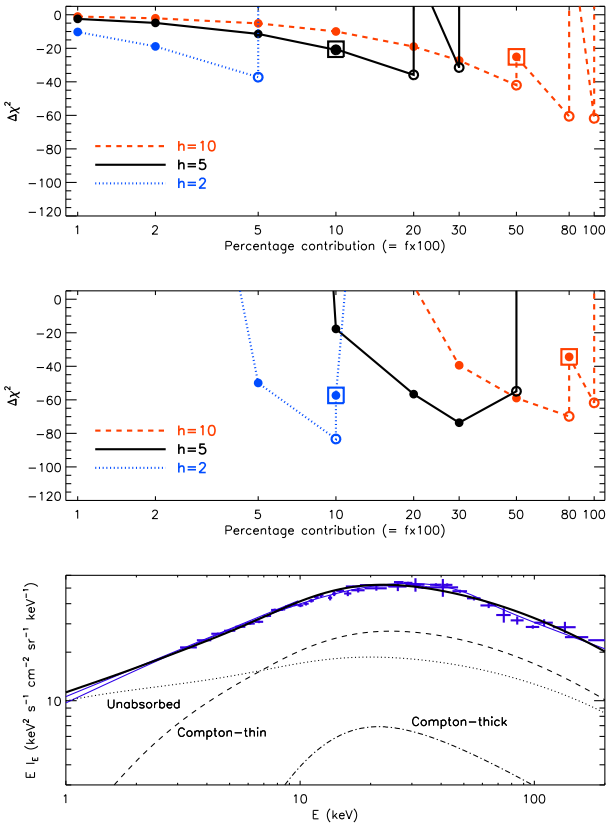


Fig. 3. **(***Top:)* $\Delta\chi^2$ for the acceptable models incorporating light bending with different percentage contributions ($f \times 100$) of light bending. The change in $\chi^2$ is computed with respect to the base PEXRAV model with no light bending included. Empty circles represent solutions in which the best-fit fraction of Compton-thick sources ($r_{\rm CT}$) is small ($< 0.5$). In these cases, a secondary fit was carried out by forcing $0.5 \leq r_{\rm CT} \leq 2$ (boxed circles), which results in the apparent jaggedness of the otherwise-smooth $\Delta\chi^2$ curves. **(***Middle:)* Same as above, but with reflection-free (i.e. PEXRAV-free) power-law SEDs that incorporate different percentage contributions ($f \times 100$) of light bending. **(***Bottom:)* Best-fit modelled XRB spectrum for one of the solutions ($h$=5, $f$=0.3) incorporating PEXRAV-free power-laws+light-bending. The data is from Gruber et al. (1999).

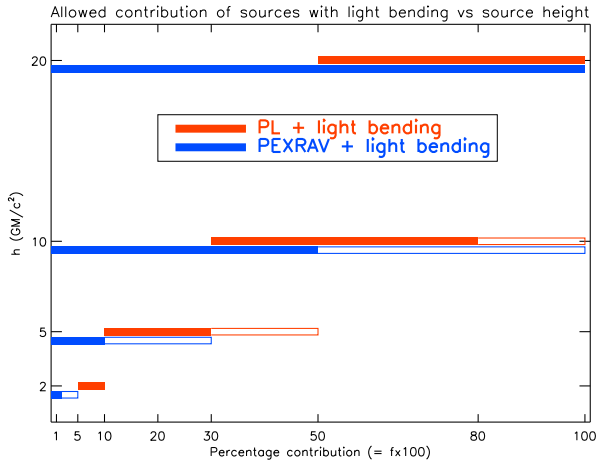


Fig. 4. Allowed combinations of ($f$, $h$) determined by fitting light-bent SEDs to the XRB, as described in the text. At each height $h$, the lower, blue bar denotes the 'PEXRAV+light bending' scenario (Fig. 3, *top*) and the red, upper bar is for the ' PL+light bending' scenario (Fig. 3, *middle*). Acceptable solutions that require a small Compton-thick fraction ($r_{\rm CT}$<0.5) are outlined by the empty bars, the rest being denoted by the filled bars. Though bars are drawn continuously for clarity, only the discrete $f$ values of the previous figures were investigated.

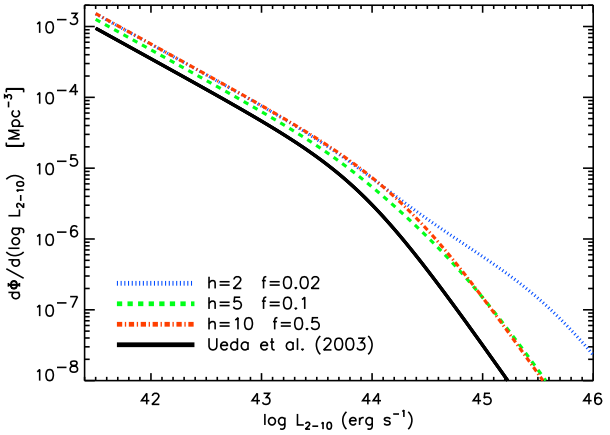


Fig. 5. Determination of XLFs based on *intrinsic*, rather than observed, flare luminosities. The black solid line shows the base 2–10 keV XLF from U03, i.e. without correction for light bending. The other lines show the XLF for $L_{2-10} = L_{\rm flare}$, using some maximum best-fit $f$ values at each $h$ for the case of *i)* PEXRAV + light bending scenario. The redshift of $z = 0.1$ is simply chosen as the 'local' example (cf. Fig 11 of U03). With increased light bending at low $h$, the correction to intrinsic luminosities goes up; or equivalently, the source number density at any given luminosity is increased.

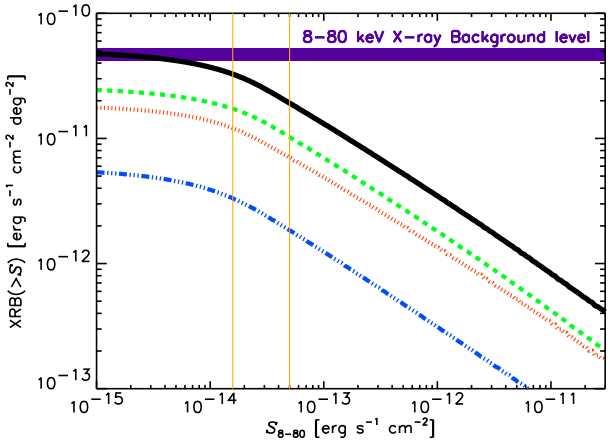


Fig. 6. The cumulative 8–80 keV XRB expected to be resolved by $NeXT$, as a function of flux. The width of the blue band near the top denotes the normalization uncertainty in the observed XRB: between 1 and 1.26 × the background level inferred from the fit of Gruber et al. (see discussion in U03). The thin yellow vertical lines are drawn at representative 100 ks and 1 Ms flux limits of 5 and 1.6 $\times 10^{-14}$ erg s$^{-1}$ cm$^{-2}$. From top to bottom, the cumulative model XRB curves are i) the contribution of all sources (solid black); ii) that of Compton-thin obscured AGN (green dashed); iii) unobscured AGN (red dotted); and iv) Compton-thick AGN (blue dot-dashed).